algorithms

MDPI

Article

Study of the Algorithm for Wind Shear Detection with Lidar Based on Shear Intensity Factor

Shijun Zhao and Yulong Shan *

School of Meteorology and Oceanography, National University of Defense Technology, Nanjing 210000, China; zhaoshijun17@nudt.edu.cn

* Correspondence: shanyulong18@nudt.edu.cn; Tel.: +86-13260786710

Abstract: Low-level wind shear is a vital weather process affecting aircraft safety while taking off and landing and is known as the "aircraft killer" in the aviation industry. As a result, effective monitoring and warning are required. Several ramps detection algorithms for low-level wind shear based on glide path scanning of lidar have been developed, including double and simple ramp detection, with the ramp length extension and contraction strategies corresponding to the algorithm. However, current algorithms must be improved to determine the maximum shear value and location. In this paper, a new efficient algorithm based on the shear intensity factor value is presented, in which wind speed changes and distance are both considered when calculating wind shear. Simultaneously, the effectiveness of the improved algorithm has been validated through numerical simulation experiments. Results reveal that the improved algorithm can determine the maximum intensity value and wind shear location more accurately than the traditional algorithm. In addition, the new algorithm improved the detection ability of lidar for weak wind shear.

Keywords: wind shear; ramp detection algorithm; numerical simulation; lidar

Citation: Zhao, S.; Shan, Y. Study of the Algorithm for Wind Shear Detection with Lidar Based on Shear Intensity Factor. *Algorithms* **2022**, *15*, 133. https://doi.org/10.3390/a15040133

Academic Editor: Mihaly Mezei

Received: 26 February 2022
Accepted: 9 April 2022
Published: 18 April 2022

1. Introduction

Wind shear is defined as the change of the wind speed vector between two points in space along a certain direction. When the wind shear occurs below 1600 ft, it means that when the low-level wind shear occurs [1,2], it can easily cause flight accidents [3,4] due to changes in the dynamic performance of aircraft and an insufficient response time for the pilot. Therefore, low-level wind shear could seriously affect the safety of aircraft takeoff and landing. According to data from the National Transportation Safety Commission of the United States, low-level wind shear has been responsible for more than 80% of fatal air accidents in the United States since 1975 [5]. Therefore, low-level wind shear is also known as the "aircraft killer" in the aviation industry [6]. Currently, the number of airports with a Low-Level Wind Shear Alert System (LLWAS) in China is very low [7]. With the increasing number of airports and more frequent aviation activities in China, studies on low-level wind shear monitoring and early warning have important practical implications and application prospects.

The technology of wind shear monitoring and early warning mainly involves two aspects: the accurate acquisition of wind field information and the detection algorithm for wind shear based on the obtained wind field data. To acquire wind field data, many devices have been developed and lidar has numerous advantages over traditional wind detection equipment. The data from lidar have a higher space-time resolution and can also be used for wind field detection in the clear sky. Lidar can also realize the high space-time resolution and high-precision detection for the slide of aircraft path, making up for the shortcomings of traditional wind measurement equipment. At this time, lidar has been widely used in flight meteorological support at large international airports abroad [8]. Therefore, this paper studies the improvement of the alerting algorithm for low-level wind

shear with lidar. At present, many alerting algorithms for low-level wind shear with lidar have been proposed to alert wind shear according to the energy change of aircraft in the wind field, including the F-factor algorithm [9] and the modified F-factor algorithm [10]. In addition, an algorithm to alert wind shear by calculating the eddy current dissipation rate has been put forward [11]. The least-square fitting algorithm [12] and 8-neighborhood algorithm [13] can also be used for wind shear monitoring.

Hong Kong Observatory's Chan and Shun et al. proposed the slide path scanning (SP) method based on lidar and designed the ramp detection algorithm for wind shear [12,14]. To find the maximum shear intensity and location, the algorithm extends and contracts the detection (ramp) length according to the changing wind speed trend. The algorithm has been successfully applied to the Hong Kong International Airport, with the hit rate for wind shear being 76%. However, this algorithm only uses the changing trend of wind speed to adjust the ramp length when determining the maximum shear position, but the wind shear intensity is affected by the changing trend of the wind speed and the ramp length itself. Therefore, adjusting the ramp length based on the changing wind speed trend cannot detect the value and position of maximum shear alone.

Jiang and Xiong et al. improved the ramps detection algorithm [15] and F-factor algorithm [10], respectively. The conventional single ramp detection was improved to a double ramps' detection algorithm. The new algorithm not only calculates the shear value along the ramp, but also calculates the difference between the shear values on two adjacent single ramps. The final result is combined with the detection results of single and double ramps. The improved algorithm can effectively improve the accuracy of wind shear detection. However, ramp length extension and contraction strategy have not been improved. For the F-factor algorithm, they found the relationship between the vertical wind speed and the wind speed gradient along the slide path through mathematical derivation and eliminated the vertical wind speed term. The results revealed that the modified F-factor algorithm has a better detection performance for small-scale wind shear. However, the determination of the alarm threshold still needs further research. For the Plane Position Indicator (PPI) scanning mode of lidar, Jiang Lihui et al. proposed the gradient search alerting algorithm of low-level wind shear based on a spatial adaptive scale [16]. The core idea of this algorithm is to calculate the velocity gradient based on several spatial adaptive scales, with the best fitting scale depending on the wind shear intensity factor. The results demonstrated that the algorithm could detect wind shear of all spatial scales and improve the alarm rate. Lanqian Li et al. [17] designed a new slide path wind shear detection algorithm based on the PPI scanning method of lidar and improved the calculation of wind profile along the slide path. Results showed that their algorithm could successfully identify low-level wind shear, achieving a 94% alerting rate compared to 88% for the conventional ramp detection algorithm based on the same dataset. However, their algorithm has still not improved the extension and contraction strategy of ramp length.

In conclusion, the currently proposed wind shear alerting algorithms can be divided into two main types. One uses the correlation factors of wind shear, such as the F-factor algorithm and eddy dissipation rate, to monitor wind shear. Another directly monitors the wind field data's intensity and wind shear location based on the concept of wind shear itself. To accurately determine the intensity and location information of wind shear, this paper improved the ramp extension and contraction strategy in the ramp detection algorithm based on the wind shear intensity factor and tested the effectiveness of the improved algorithm by numerical simulation. Due to the complicated weather during wind shear, it is difficult to directly measure the real intensity and location of wind shear. Therefore, the wind shear data in the pilot's report are generally used as the true values. However, the pilot's report is subjective and the wind shear event is generally found afterwards, so data from the pilot's report are usually inaccurate, meaning the wind shear intensity depends on this subjective judgment. At the same time, if wind shear is detected at the airport, the aircraft is usually not allowed to take off and land. So, the wind shear data in the pilot's

report are very limited. Therefore, simulating the wind shear wind fields to verify the effectiveness of wind shear detection algorithms is necessary.

This paper is organized as follows. Section 2 describes the methods used for the working principle of conventional and improved algorithms and the technical process of the paper. Section 3 discusses the numerical simulated experiments and presents the results. The final section (Section 4) provides discussion and presents the conclusions.

2. Methods

2.1. Glide Path Scanning and Headwind Data Acquisition

Glide path scanning focuses on the detection of wind field information along the glide path and identifies wind shear within this range [18]. The glide path is the flight trajectory of an aircraft during take-off and landing. As shown in Figure 1, to ensure the laser beam is always able to scan the glide path, the elevation and azimuth of the lidar system components need to change simultaneously when scanning the glide path. Since the angle between the glide path and the runway is 6° during take-off and 3° during landing, different elevation angle changes should be set according to the aircraft's take-off and landing state. Compared with the traditional PPI scanning method, the glide path scanning method has a smaller azimuth angle change range and requires fewer laser beams, so the scanning period is shorter and the efficiency is greatly improved. The data points closest to the glide path are seen as the data in the glide path at that height, so that the headwind on the glide path can be obtained in this way. When the lidar is installed on the landing point, lidar only needs to scan once to obtain the headwind on the glide path. Note that the wind data used for the improved algorithm here are headwind data, which is the wind speed in the direction of the glide path. Therefore, although wind direction is the important parameter when calculating wind shear [19], wind direction is not considered when calculating wind shear information in this paper.

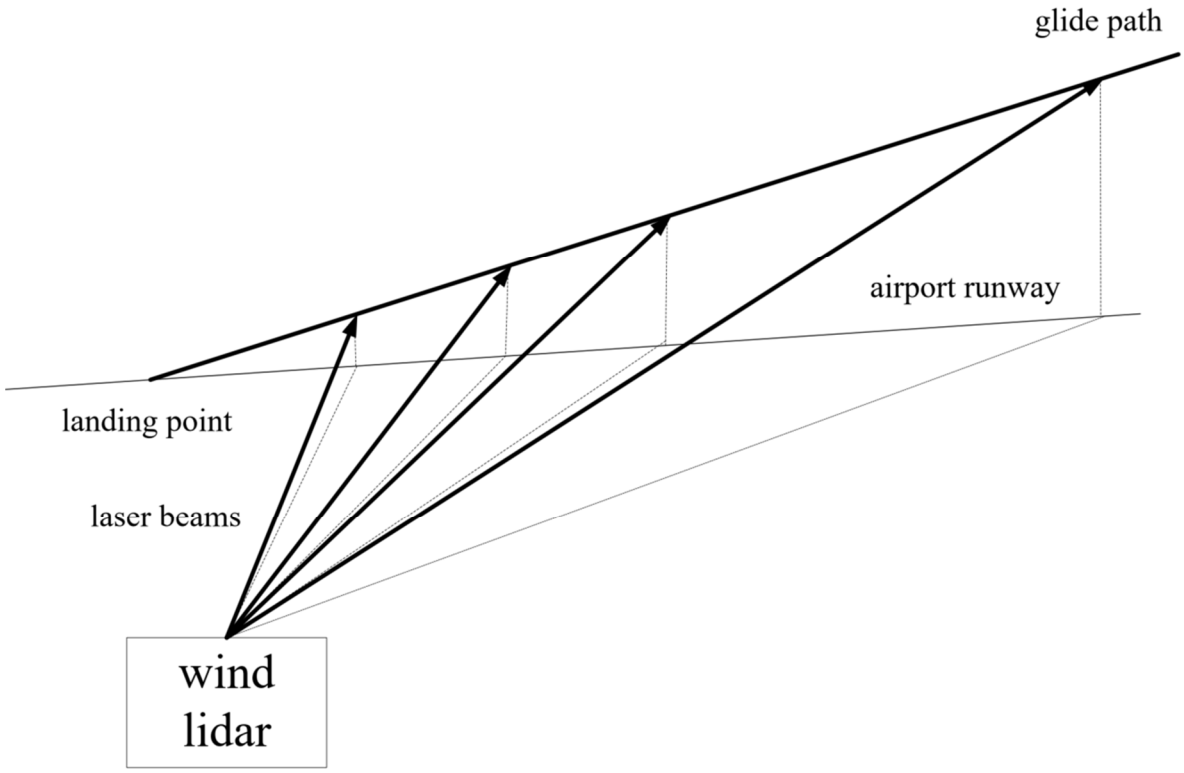

Figure 1. Schematic diagram of glide path scanning.

2.2. Conventional Single Ramp Wind Shear Detection Algorithm

The principle of a single ramp detection algorithm, which detects the change of wind speed at a certain distance, is presented in Figure 2. Since the wind speed at both ends of the detection distance varies, the wind profile along the slide path is reflected as a ramp. Therefore, the algorithm is named the ramp detection algorithm.

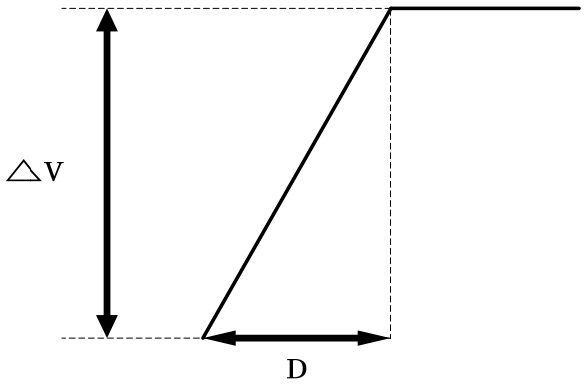

Figure 2. The principle of the conventional single ramp wind shear detection algorithm.

Here, D is the length of the ramp, which represents the distance of the two data points, and ΔV is the difference in wind speed between the two data point locations.

Since noise data may exist in the original data of the headwind profile, it is necessary to filter the original wind profile before ramp detection. An average sliding method is generally used to preprocess the raw wind data. Based on the sliding average algorithm, we define U as the raw wind profile data and UI as the preprocessed wind profile data. The equation of sliding average is given below. Note that the sliding average algorithm is referring to the data averaged spatially and wind profile is referring to headwind data.

$$\mathrm{UI(d)} = \frac{1}{4}\mathrm{U(d-\Delta d)} + \frac{1}{2}\mathrm{U(d)} + \frac{1}{4}\mathrm{U(d+\Delta d)} \tag{1}$$

Here, d is the location of the data point to be preprocessed and Δd is the sampling distance.

The preprocessed wind profile could be used to detect wind shear, with the equation for detecting wind shear as follows:

$$\mathrm{UID}\left(\widetilde{\mathrm{d}}\right) = \mathrm{UI(d+D)} - \mathrm{UI(d)} \tag{2}$$

Here, UID ($\widetilde{\mathrm{d}}$) is the wind shear in location $\widetilde{\mathrm{d}}$ and $\widetilde{\mathrm{d}}$ = d + D/2, where D is the length of the ramp.

Interestingly, if D is fixed, the algorithm cannot find the maximum wind shear value and location when the changing trend of wind speed in the ramp is the same as that on the next point outside the ramp. Therefore, extending or contracting the ramp length is necessary based on specific criteria. Bowei Chen et al. put forward the ramp length extension and contraction strategy as depicted in Figure 3.

For a ramp of headwind gain (loss), if the velocity continues to rise (fall) after the original ramp, the ramp length is expanded to cover the increasing (decreasing) part of the velocity until the velocity starts to fall (rise) or half of the original ramp length is reached, whichever is shorter. On the other hand, for a ramp of headwind loss (gain), if velocity increases (decreases) at the final portion of the ramp, the ramp length is contracted until the increasing (decreasing) part of the velocity is passed or a quarter of the original ramp length is reached, whichever is smaller.

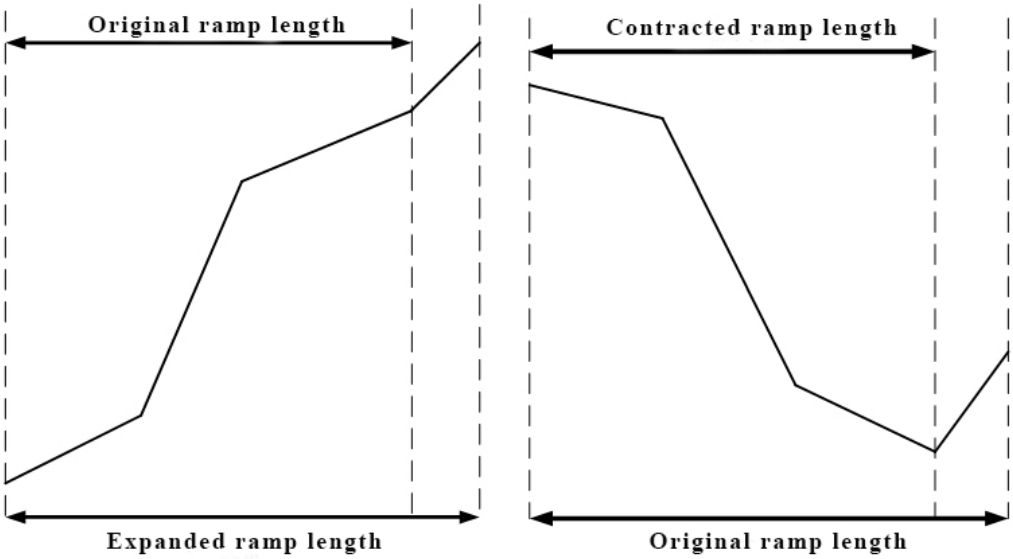

Figure 3. The principle of the ramp length extension and contraction strategy of conventional single ramp wind shear detection algorithm.

The double ramps detection algorithm calculates the difference in wind shear at adjacent locations based on the single ramp detection algorithm under the condition of fixed ramp length. When the difference in wind shear at adjacent locations is higher than the prespecified threshold, wind shear alerting information is also released. Since this paper focuses primarily on the ramp length extension and contraction strategy, the double slope detection algorithm is not described in detail here.

2.3. Improvement of Ramp Length Extension and Contraction Strategy

The value of wind shear itself reflects the change of wind speed at a certain distance. However, the impact of wind shear on a flight depends not only on the change of wind speed, but also on the ramp length corresponding to the change of wind speed. If the change of wind speed is significant and the corresponding ramp length is small, the wind shear could significantly impact the flight. However, if the change of wind speed is significant and the corresponding ramp length is also large enough, the impact of wind shear on the flight is likely to be small. Therefore, the ramp length determined only based on the change of wind speed itself cannot effectively find the location that has a high impact on flight safety.

Woodfield and Woods put forward the concept of wind shear intensity factor in 1983 [20], and their definition considered the variability of wind speed and the corresponding ramp length simultaneously, which can more objectively reflect the impact of wind shear on the flight. The wind shear intensity factor can be defined as follows:

$$S = \left(\frac{dV}{dt}\right) g \left(\frac{\Delta V}{V_a}\right)^2 = \left(\frac{\Delta V}{R^{1/3}}\right)^3 g V_a^{-1} \tag{3}$$

where dV/dt represents the change rate of wind speed; ΔV represents the variation of wind speed; V_a represents the aircraft's approach speed when landing, which is usually constant, but different aircraft's V_a varies; and R represents the ramp length corresponding to ΔV.

It can be noted from Equation (3) that the contribution of the total change in the degree of wind speed to the wind shear intensity factor is greater than that of the wind speed's change rate. This may explain why the traditional ramp detection algorithm only releases the wind shear alert based on the total change value of wind speed. Considering that the approach speeds of different aircraft vary during landing, this paper simplifies the calculation of the wind shear intensity factor. The simplified wind shear intensity factor

S_{simple} is defined as follows. Note that the wind shear intensity factors mentioned below all refer to S_{simple}

$$S_{simple} = \frac{\Delta V^3}{R} \tag{4}$$

Since the wind shear intensity factor can better reflect the impact of wind shear on flight safety, this paper improved the ramp detection algorithm by determining the best ramp length based on the wind shear intensity factor. Concurrently, the ramp length determined only based on the changing trend of wind shear intensity within the length range of a single ramp cannot guarantee its global optimality. For example, we assume that the wind shear intensity gradually increases within the range of ramp length D. In that case, the wind shear intensity in the location of data point D + L1 decreases, while in the location of data point D + L2 it continues to increase. At the same time, the wind shear intensity in the location of data point D + L2 is higher than that within the range of D. The wind shear intensity in D + L2 is the maximum value of all data points. At this time, if the final ramp length is determined only based on the changing trend of wind shear intensity within the range of a single ramp, the ramp length should be D, but the real optimal ramp length is D + L2 (Figure 4). Therefore, the optimal ramp length determined only based on the changing trend of wind shear intensity within the range of a single slope cannot guarantee its global optimality.

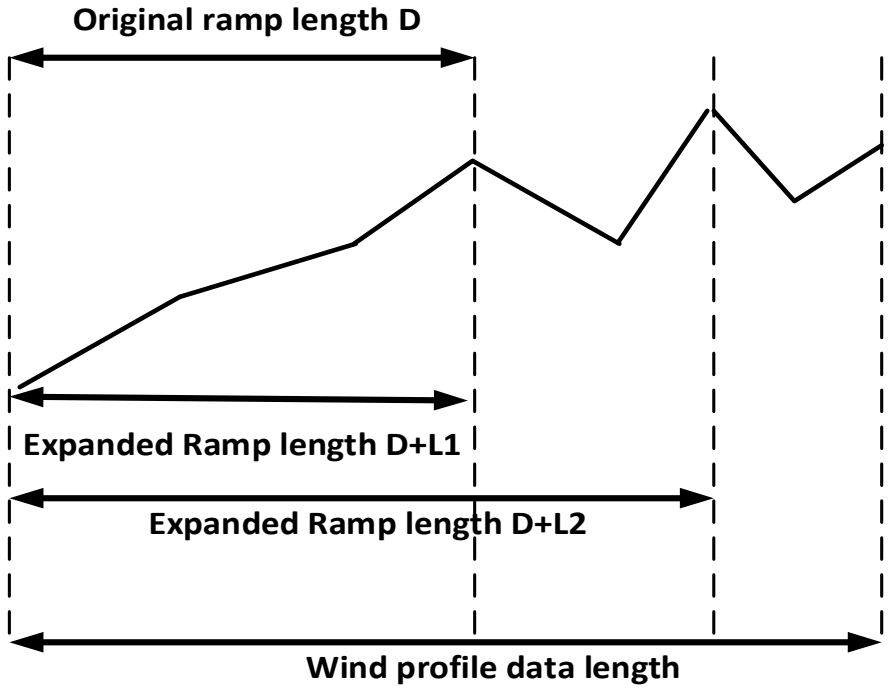

Figure 4. The principle of the improved ramp length extension and contraction strategy single ramp wind shear detection algorithm.

For the problems described above, this paper proposed the following ramp length determination strategy: calculate the wind shear intensity of any data point relative to all other data points and then find the data point with the highest wind shear intensity of each data point relative to all other data points, and finally determine the optimal ramp length of each data point and its corresponding wind shear intensity. Theoretically, the new algorithm can obtain the maximum wind shear intensity and location of the used wind profile data better than the traditional ramp length adjustment strategy.

2.4. Framework of the Project

This paper tested the feasibility of the improved algorithm by detecting wind shear in the simulated wind field. First, construct the three-dimensional simulated wind field under four weather conditions, then determine the location of lidar and slide path in the three-dimensional coordinate system of the simulated wind field. Then, simulate the lidar scanning the slide path, calculate the radial wind speed of the lidar at the slide path according to the elevation angle of the laser beam and further obtain the headwind profile. Next, calculate the wind shear intensity and position with the conventional and improved single ramp detection algorithms and double ramp detection algorithm. Finally, compare the calculated wind shear results of the three algorithms and analyze the advantages and disadvantages of each. The framework of this paper is displayed in Figure 5. It must be noted that the improved single ramp wind shear detection algorithm in this paper is Wind Shear Detection based on Severity Factor (WSDSF), while the conventional single ramp wind shear detection algorithm is Wind Shear Detection based on Headwind Profile (WSDHP).

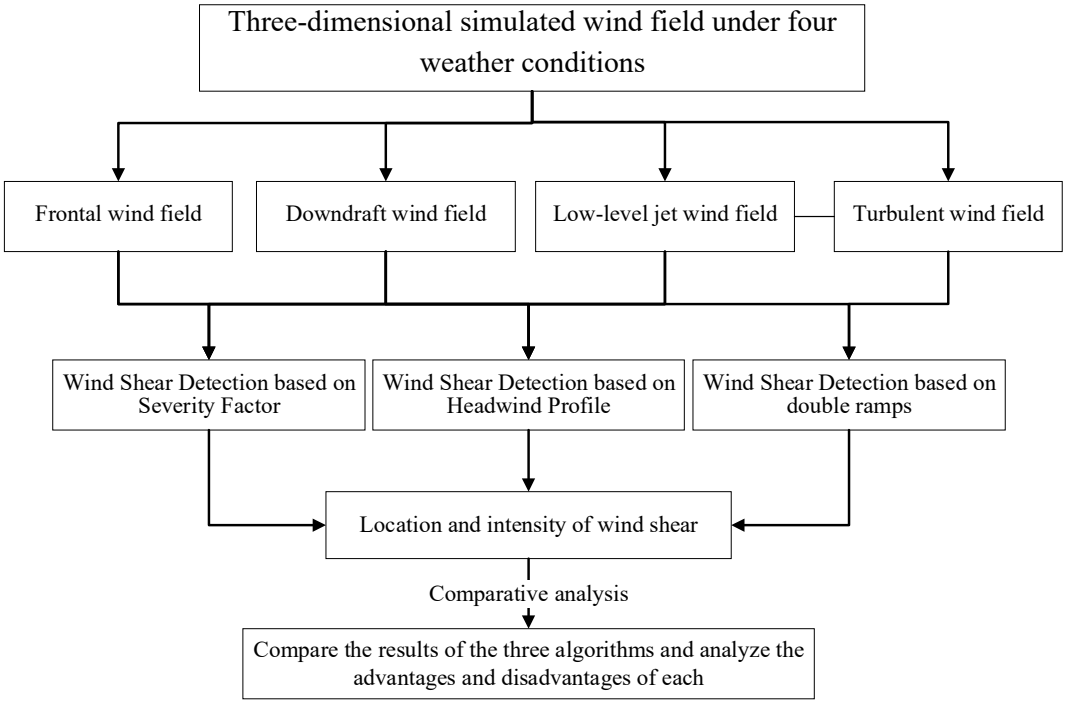

Figure 5. Framework of the project in this paper.

3. Test of the Improved Algorithm Based on Numerical Simulation

Four typical wind fields with wind shear are simulated based on MATLAB toolbox (Natick, MA, USA), including frontal wind field, downburst wind field, low-level jet wind field and turbulent wind field. Lidar is simulated to scan the slide path in the four simulated wind fields, then we can use the simulated lidar data and different wind shear detection algorithms to detect the wind shear in the four simulated wind fields. In this way, we can reasonably compare the effectiveness of different algorithms in wind shear detection. In the numerical simulation, the position of lidar is set to be the same as the landing point of the slide path; the elevation angle of the laser beam and slide path are both set to be 30°; the azimuth angle of the laser beam is set to be 45°′ the range resolution of lidar is set to be 1000m; and the simulated wind field is limited to a space area of 10,000 × 10,000 × 10,000 m^3.

According to the standard of wind shear intensity from the International Civil Aviation Organization (ICAO), when the wind shear intensity value is between 0 and 0.07 S^{-1}, it is rated as mild wind shear. When the wind shear intensity value is between 0.08 S^{-1} and 0.13 S^{-1}, it is rated as moderate wind shear; when the wind shear intensity value is between

0.14 S^{-1} and 0.20 S^{-1}, it is rated as strong wind shear; when the wind shear intensity value is greater than 0.20 S^{-1}, it is rated as severe wind shear. The wind shear intensity factor value S_{simple}, which corresponds to the standard of ICAO, can be calculated based on the wind shear intensity values, which are shown in detail in Table 1.

Table 1. The standard of wind shear intensity and its corresponding wind shear intensity factor value recommended by ICAO.

Strength Grade	The Standard of Windshear Intensity		Effect on Flight Safety
	Windshear Intensity (S^{-1})	Windshear Intensity Factor ($\frac{m^2}{s^3}$)	
Mild	0–0.07	0–0.27	The track and airspeed of aircraft changes slightly
Moderate	0.08–0.13	0.28–2.13	May make the operation of aircraft difficult
Strong	0.14–0.20	2.14–7.20	May lead to loss of control of aircraft
Severe	>0.20	>7.20	May cause serious harm

3.1. Frontal Wind Field

The front is the weather system formed when cold and warm air masses meet. Since the density of cold air is greater than that of warm air, the warm air will rise along the cold air to form an inclined junction area when the two air masses meet, forming wind-direction-shear and wind-speed-shear at the interface. The constructed simulated frontal wind field is depicted in Figure 6. The red straight line in Figure 6 is the simulated aircraft's slide path and laser beam in slide path scanning. The simulated wind field comprises two air masses with two opposite motion directions, with the simulated wind speed being 10 m/s. The wind direction of the lower air mass tilts 45° to the positive direction of the *Z*-axis, while the wind direction of the upper air mass is 45° to the negative direction of the *Z*-axis. Wind-direction-shear and wind-speed-shear are formed at the junction of the two air masses.

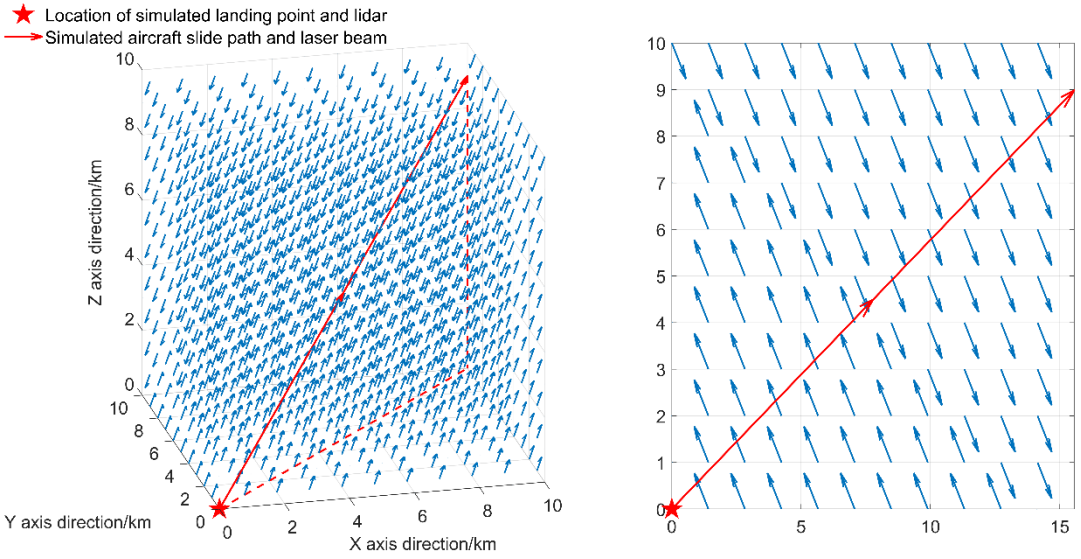

Figure 6. The left figure is the simulated frontal wind field in the 3-D coordinate system; the right figure is the profile view of the simulated frontal wind field.

The results of wind shear detection under the background of the frontal wind field are illustrated in Figure 7, where the black dotted line represents the headwind profile data in the slide path obtained by the simulated lidar. The results reveal that wind shear existed at the data acquisition point within 8500–9000 m of the aircraft landing point. Here, the

wind speed changes by 2.25 m/s within a 500 m distance and the shear intensity factor value is 0.02, which is assumed as mild wind shear. At this time, both algorithms WSDSF and WSDHP can detect this weak wind shear, and the calculated wind shear intensity and position are consistent with the actual case. Concurrently, the double ramps detection algorithm also realizes the warning of wind shear. However, the calculated position of wind shear is different from the actual case, and the calculated wind shear intensity is higher than the actual wind shear intensity. In this experiment, WSDSF and WSDHP perform better than the double ramps detection algorithm.

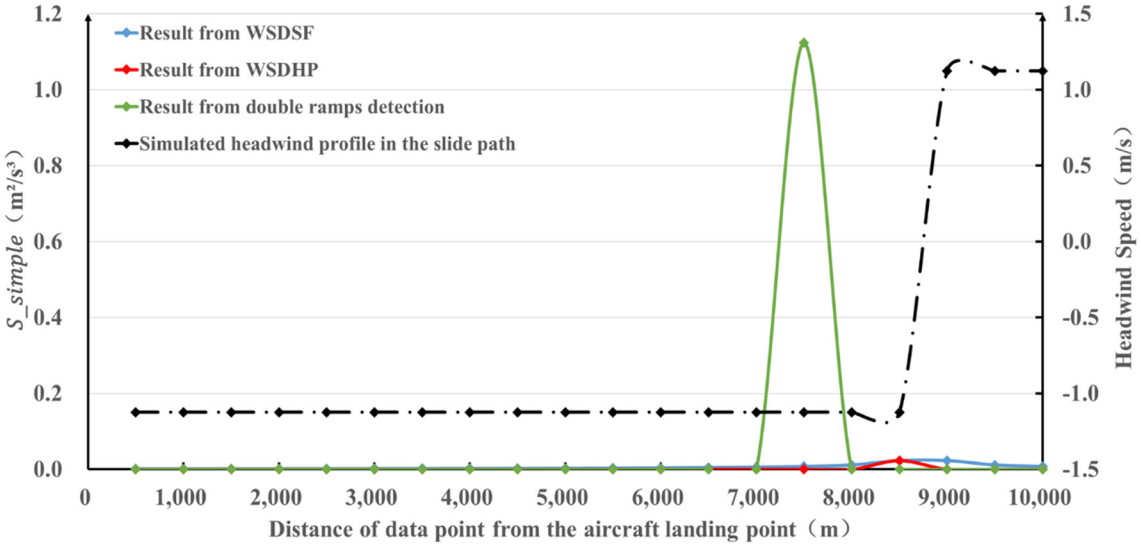

Figure 7. The results of wind shear detection under the background of the frontal wind field.

3.2. Downdraft Wind Field

A downburst is a strong convective weather phenomenon [21]. It is a strong downdraft usually generated in thunderstorm clouds. When the aircraft passes a downburst, it will encounter a sudden change of wind direction and its altitude could drop rapidly. Therefore, it is very easy for an accident to occur when the aircraft passes a downburst. The simulated wind field of a downburst in this paper is displayed in Figure 8, where the downdraft speed and its adjacent diffusion airflow speed are both set as 50 m/s and the surrounding airflow is set as turbulent wind field. Note that the height of the simulated downdraft wind field is higher than the actual height. Since the experiment is to test the effectiveness of the improved algorithm on wind shear detection in the wind field with the characteristic of downdraft, it does not influence the experiment's purpose. The red straight line in Figure 8 is the slide path and laser beam of the simulated aircraft in slide path scanning.

The results of wind shear detection under the background of the downdraft wind field are depicted in Figure 9, where the black dotted line represents the headwind profile data in the slide path obtained by the simulated lidar. The results revealed that wind shear exists at multiple positions. Algorithm WSDHP finds the wind shear at multiple locations. Among the results from algorithm WSDHP, the strongest wind shear is located 5000 m away from the aircraft landing point and the maximum wind shear intensity factor value is 19.35. The second-strongest wind shear is located 7000 m away from the aircraft landing point and the wind shear intensity factor value is 15.63. Algorithm WSDSF also finds wind shear at multiple locations, with the calculated maximum wind shear positions the same as the result of algorithm WSDHP. However, the calculated maximum wind shear intensity value of 55.74 is much larger than that calculated from the algorithm WSDHP. Concurrently, it is interesting that the wind shear intensity value 7000 m from the aircraft landing point is the same as that at 5000 m. In addition, both algorithms can accurately detect the position of maximum wind shear, but the maximum wind shear intensity values calculated differ due to the different ramp lengths of the two algorithms. Therefore, it can be concluded that the

wind shear intensity value calculated based on the ramp length from algorithm WSDSF is larger than that from algorithm WSDHP, and algorithm WSDSF can more accurately detect the position of maximum wind shear and the real wind shear intensity at each position. Concurrently, the double ramps detection algorithm also found the wind shear at multiple locations and accurately determined the location of the maximum wind shear. However, it should be noted that the wind shear intensity from the double ramp detection algorithm is much smaller than that from algorithms WSDHP and WSDSF, which did not accurately reflect the real wind shear intensity at each location. It can be concluded that the double ramp wind shear detection algorithm easily underestimated the wind shear intensity when the real wind shear was strong.

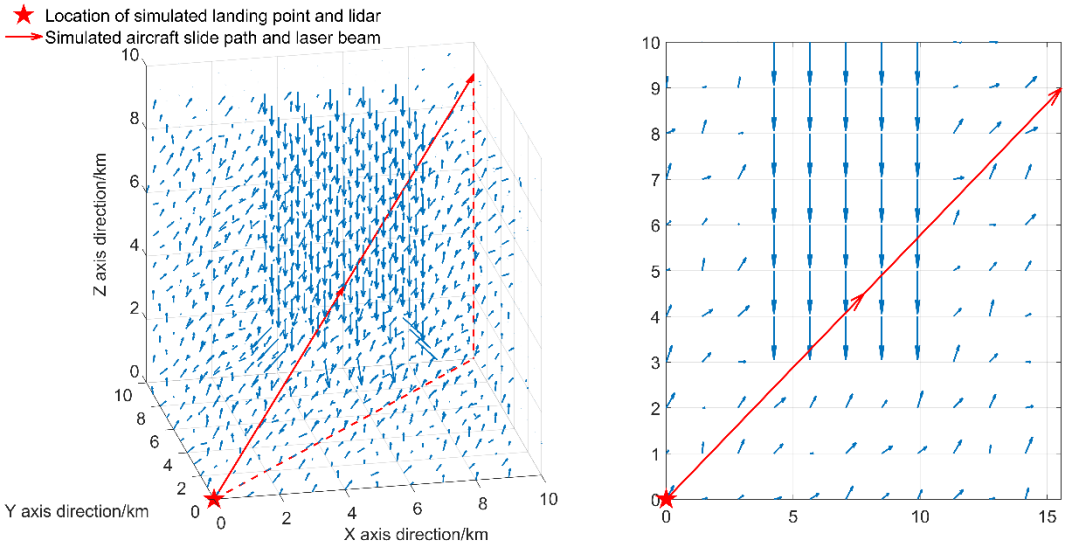

Figure 8. The left figure is the simulated downdraft wind field in the 3-D coordinate system; the right figure is the profile view of the simulated downdraft wind field.

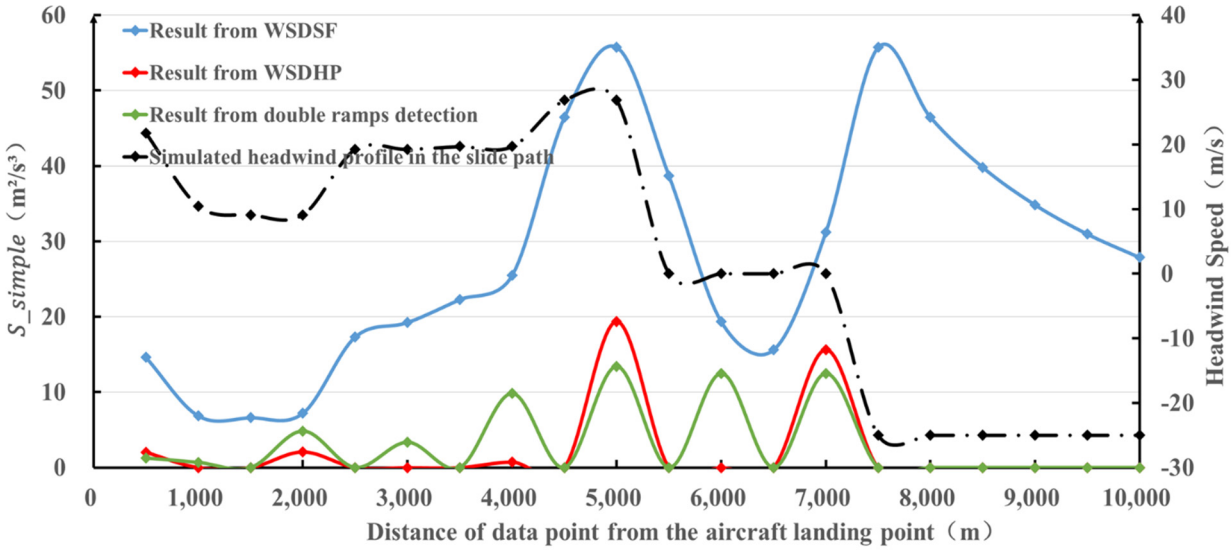

Figure 9. The results of wind shear detection under the background of the downdraft wind field.

3.3. Low-Level Jet Wind Field

A low-level jet is the strong, narrow airflow zone in the boundary layer or lower troposphere [22]. The wind speed is highest in the center of the airflow zone and lowest in the upper and lower layers, causing vertical wind speed shear. The simulated low-level jet wind field is displayed in Figure 10. To better conduct the numerical simulation

experiments and compare the results of the three algorithms in the four wind fields, the size of the 3-D coordinate system for the space used is fixed. The simulated height of the low-level jet is higher than the actual conditions, which does not influence the experiment's purpose. Therefore, in the simulated low-level jet wind field, the maximum wind speed exists in the height range of 4000 to 5000 m, set at 40 m/s. The minimum wind speed exists at the height of 3000 m and below, at 5 m/s; the wind speed at 6000 m and above is set as 10 m/s. The red straight line in Figure 10 is the slide path and the laser beam of the simulated aircraft in slide path scanning.

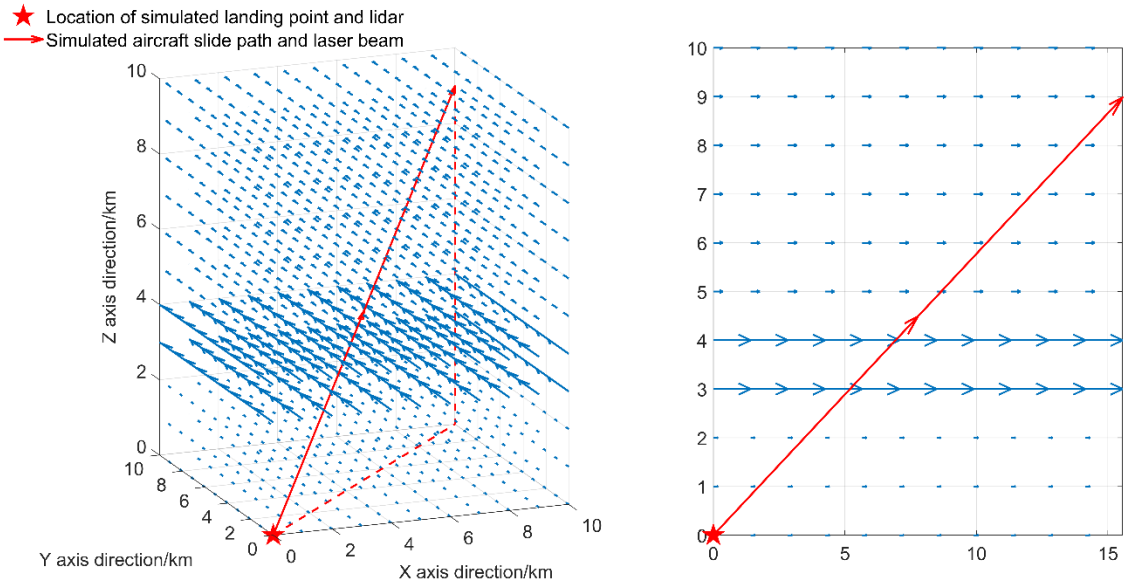

Figure 10. The left figure is the simulated low-level jet wind field in the 3-D coordinate system; the right figure is the profile view of the simulated low-level jet wind field.

The results of wind shear detection under the background of a low-level jet wind field are shown in Figure 11, with the black dotted line representing the headwind profile data in the slide path obtained by the simulated lidar. The results reveal that the wind shear mainly exists between 5000 and 9000 m from the aircraft landing point. The algorithm WSDHP accurately identified the position of maximum wind shear, which occurred 5000 m from the aircraft landing point, and its wind shear intensity factor value was 19.69. The second maximum wind shear intensity factor was 6.2 and occurred 9000 m away from the aircraft landing point. In addition, WSDSF accurately identified the position of maximum wind shear, and its wind shear intensity factor value was 19.69, which is the same as the result of algorithm WSDHP. However, the wind shear intensity factor calculated by algorithm WSDSF at 9000 m from the aircraft landing point was 12.4, which is higher than algorithm WSDHP. Therefore, it can be further concluded that the ramp length calculated by algorithm WSDSF can more accurately identify the position of maximum wind shear and the real wind shear intensity value at each position. The double ramp detection algorithm also accurately determined the position of maximum wind shear, but it issued the false warning of wind shear near 4000 and 8000 m from the aircraft landing point, as the shear intensity values at these two positions should be significantly lower than those at 5000 and 9000 m (see the headwind profile data in the slide path). This phenomena could be because the double ramp detection algorithm is sensitive to weak wind shear.

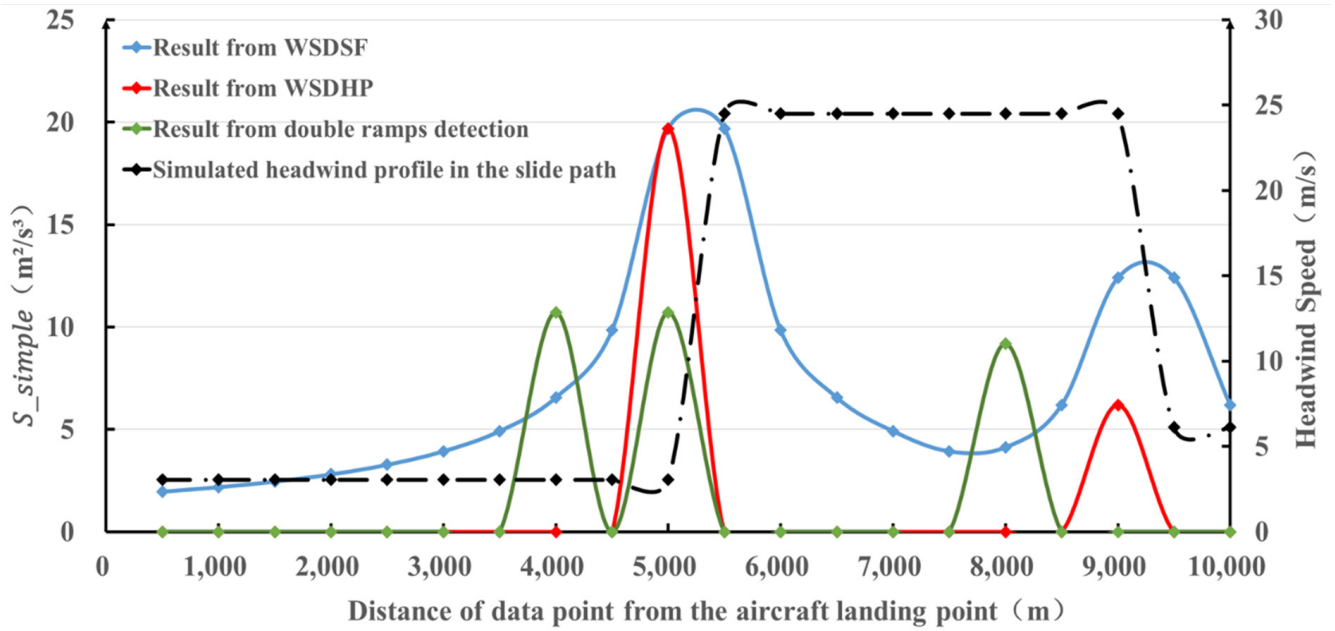

Figure 11. The results of wind shear detection under the low-level jet wind field background.

3.4. Turbulent Wind Field

Buildings, mountains, trees and other obstacles near the airport will hinder the flow of air and change the wind direction, causing an irregular turbulence of wind and affecting the takeoff and landing of aircraft. The turbulent wind field simulated in this paper is depicted in Figure 12, where the wind speed and direction change irregularly. The red straight line in Figure 12 is the slide path and the laser beam of the simulated aircraft in slide path scanning.

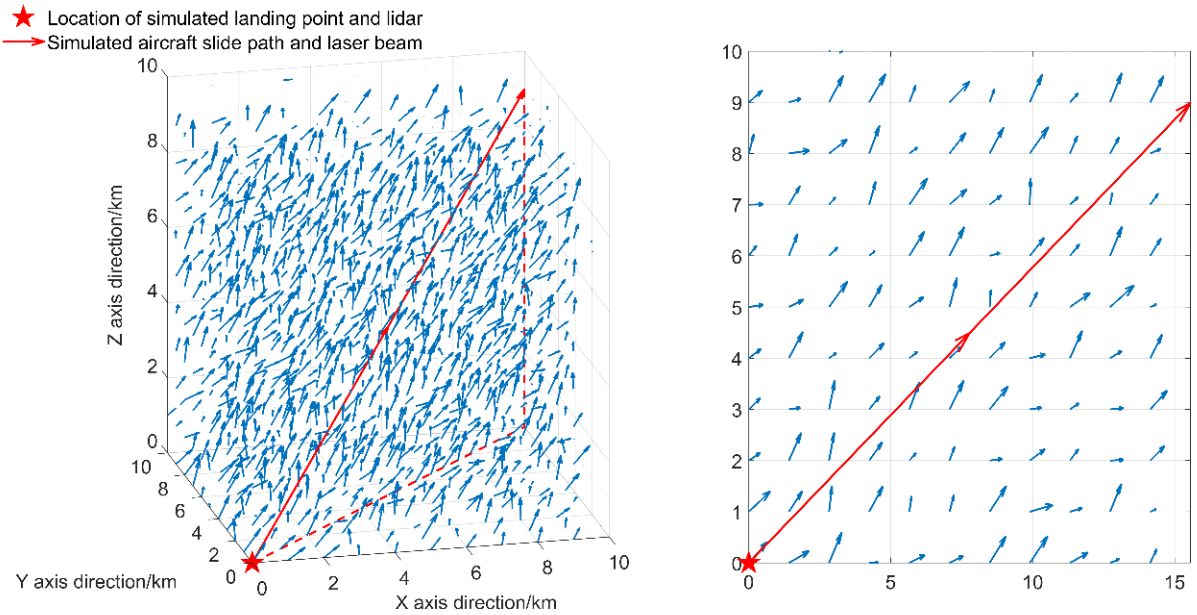

Figure 12. The left figure is the simulated turbulent wind field in the 3-D coordinate system; the right figure is the profile view of the simulated turbulent wind field.

The wind shear detection results under the turbulent wind field background are presented in Figure 13, where the black dotted line represents the headwind profile data in the slide path obtained by the simulated lidar. The results indicate that wind shear exists at multiple positions away from the aircraft landing point, but the change in the

wind speed is negligible. Simultaneously, both algorithms WSDSF and WSDHP accurately identify the maximum wind shear at 9000 m from the aircraft landing point. However, their calculated wind shear intensity factor values are small, 0.35 and 0.69, separately, and should be classified as moderate wind shear. In addition, the wind shear intensity calculated by algorithm WSDSF is slightly larger than that calculated by algorithm WSDHP. Concurrently, it should be observed that the wind shear detection results of the double ramp detection algorithm are more detailed and richer and find multiple locations with wind shear. Furthermore, the wind shear intensity value calculated from the double ramp detection algorithm is larger than that from algorithms WSDSF and WSDHP overall. As a result, the double ramp detection algorithm detects wind shear better when the wind shear intensity is low, with the maximum wind shear intensity calculated by algorithm WSDSF closer to the real result than the other two algorithms.

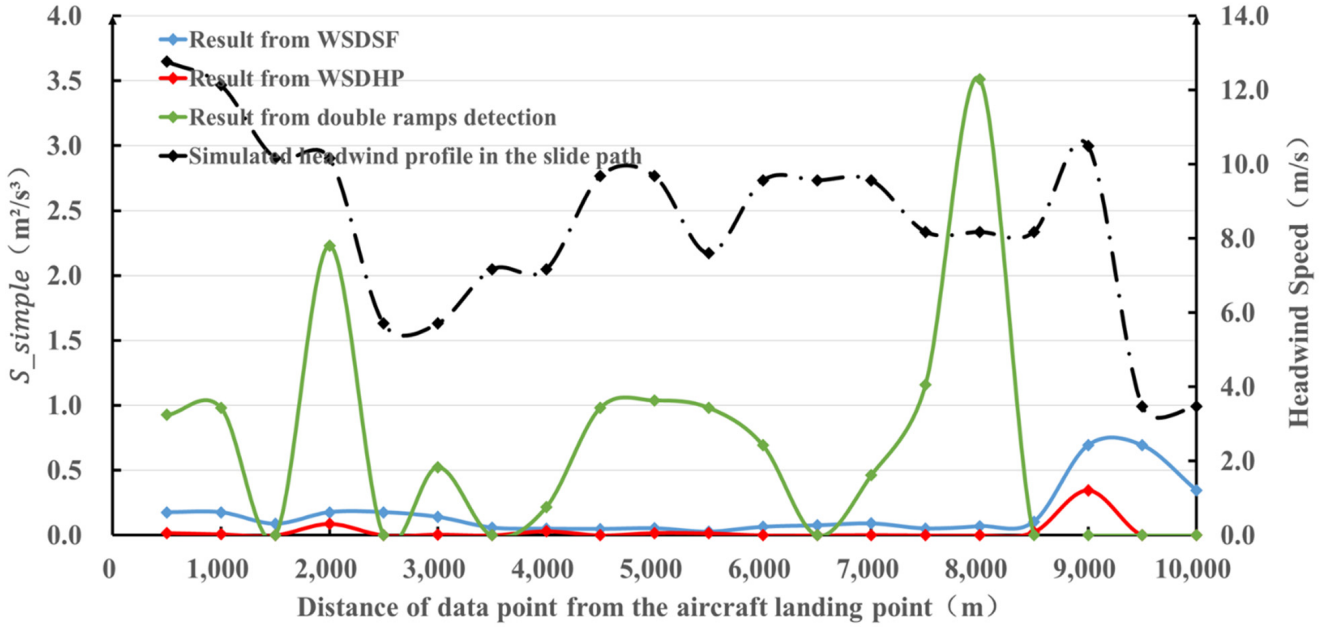

Figure 13. The results of wind shear detection under the background of the turbulent wind field.

3.5. Comparison and Analysis of the Results from the Three Algorithms under the Four Wind Winds

To better analyze the performance of the three algorithms, this paper has listed the number of wind shear alerts of different levels under different wind fields (Table 2). The results show that when the main wind shear intensity is at "Strong" and "Severe" levels, algorithm WSDSF releases the most alerts for "Strong" and "Severe" wind shear, which is due to the improved ramp length extension and contraction strategy. For example, under the downdraft wind field, algorithm WSDSF releases 18 alerts for "Severe" wind shear and 2 alerts for "Strong" wind shear. However, the double ramp detection algorithm releases 4 alerts for "Severe" wind shear and 2 alerts for "Strong" wind shear, while algorithm WSDHP only releases 2 alerts for "Severe" wind shear. When the main wind shear intensity is at "Mild" and "Moderate" levels, algorithm WSDSF still releases the most alerts for "Mild" wind shear, but the double ramp detection algorithm releases more alerts of "Moderate" and "Strong" wind shear than algorithms WSDHP and WSDSF (see the results under the frontal wind field and turbulent wind field).

Table 2. The number of wind shear alerts of different levels under different wind fields.

Wind Fields \ Algorithms		WSDSF	WSDHP	Double Ramp Detection Algorithm
Frontal wind field	Mild	7	1	0
	Moderate	0	0	1
	Strong	0	0	0
	Severe	0	0	0
Downdraft wind field	Mild	0	0	0
	Moderate	0	3	2
	Strong	2	0	2
	Severe	18	2	4
Low-level jet wind field	Mild	0	0	0
	Moderate	1	0	0
	Strong	13	1	0
	Severe	6	1	3
Turbulent wind field	Mild	20	9	1
	Moderate	0	0	9
	Strong	0	0	2
	Severe	0	0	0

4. Conclusions and Discussion

This paper improved the ramp length extension and contraction strategy of the conventional single ramp wind shear detection algorithm based on the change of wind shear intensity factor. It then tested the effectiveness of the improved algorithm by constructing the numerical simulation wind field. We then compared the wind shear detection results of the improved algorithm with the traditional single ramp and double ramp detection algorithms. Our conclusions are as follows:

(1) The conventional single ramp wind shear detection algorithm (WSDHP) can accurately locate the maximum wind shear. However, when the real optimal ramp length is long enough (generally longer than twice the distance of adjacent data point locations), the algorithm cannot accurately calculate the maximum wind shear value and the real wind shear intensity is easily underestimated.

(2) The double ramp detection algorithm is more sensitive to weak wind shear and can accurately detect it. However, it is also easy to release wrong wind shear detection results and cause an interference of wind shear warnings.

(3) The improved single ramp wind shear detection algorithm (WSDSF) can more accurately calculate the location and intensity of the maximum wind shear and provide accurate early warnings of the location and intensity of wind shear.

Overall, the improved wind shear detection algorithm has obvious advantages over the other two algorithms. However, the three wind shear detection algorithms have unique characteristics. In the factual wind shear warning service, we must combine the results of the three algorithms for our final results. In this way, we can not only verify the accuracy of the detection results based on the three algorithms, but also accurately detect the wind shear with various intensities. It is really not enough to test the effectiveness of the improved algorithm only based on numerical simulations, so further factual wind shear detection experiments are necessary in a follow-up study.

Author Contributions: Visualization, Y.S.; experimentation, S.Z.; writing—original draft preparation; S.Z. and Y.S.; writing—review and editing, Y.S. All authors have read and agreed to the published version of the manuscript.

Funding: This research received no external funding.

Data Availability Statement: Data is contained within the article.

Conflicts of Interest: The authors declare no conflict of interest.

References

1. ICAO. *Manual on Low-Level Wind Shear and Turbulence*; International Civil Aviation Organization: Montreal, ON, Canada, 2005.
2. ICAO. *Meteorological Service for International Air Navigation: Annex 3 to the Convention on International Civil Aviation*; International Civil Aviation Organization: Montreal, ON, Canada, 2007.
3. Fujita, T.T.; Caracena, F. An analysis of three weather-related aircraft accidents. *Bull. Am. Meteorol. Soc.* **1977**, *58*, 1164–1181. [CrossRef]
4. Kessler, E. Wind shear and aviation safety. *Nature* **1985**, *315*, 179–180. [CrossRef]
5. Zhao, J. *Study of Wind Shear Algorithm Based on Doppler Weather Radar Data Quality Control*; Civil Aviation University of China: Tianjin, China, 2017. (In Chinese)
6. Wang, Q.-W.; Lile, G. Development of lidar in detection of low altitude wind shear. *Laser Infrared* **2012**, *42*, 1324–1328. (In Chinese)
7. Zhao, W.; Shan, Y.; Zhao, S. Research progress of low-level wind shear detection by laser radar. *Meteorol. Hydrol. Mar. Instrum.* **2020**, *37*, 97–100+4. (In Chinese)
8. Henderson, S.W.; Hannon, S.M. Advanced coherent lidar system for wind measurements. In Proceedings of the Lidar Remote Sensing for Environmental Monitoring VI, San Diego, CA, USA, 31 July–4 August 2005; International Society for Optics and Photonics: Bellingham, WA, USA, 2005.
9. Chan, P.W. Application of LIDAR-based F-factor in windshear alerting. *Meteorol. Z.* **2012**, *21*, 193–204. [CrossRef]
10. Xing, C.; Zhen, L.; Zibo, Z. A small scale wind shear detection algorithm of modified F-factor for wind-profiling lidar. *Opt. Precis. Eng.* **2018**, *26*, 927–935. (In Chinese) [CrossRef]
11. Hon, K.K.; Chan, P.W. Application of LIDAR-derived eddy dissipation rate profiles in low-level wind shear and turbulence alerts at Hong Kong International Airport. *Meteorol. Appl.* **2013**, *21*, 74–85. [CrossRef]
12. Chan, P.W.; Shun, C.M.; Wu, K.C. Operational LIDAR-based system for automatic windshear alerting at the Hong Kong International Airport. In Proceedings of the 12th Conference on Aviation, Range, and Aerospace Meteorology, Atlanta, GA, USA, 29 January–2 February 2006.
13. Xiong, X.; Yang, L.; Ma, Y.; Zhuang, Z. Alerting algorithm of low-level wind shear based on fuzzy C-means. *J. Comput. Appl.* **2018**, *38*, 655–660. (In Chinese)
14. Shun, C.M.; Chan, P.W. Applications of an Infrared Doppler Lidar in Detection of Wind Shear. *J. Atmos. Ocean. Technol.* **2008**, *25*, 637–655. [CrossRef]
15. Jiang, L.; Yan, Y.; Xiong, X.; Chen, B.; Chen, X.; Zhang, D. Doppler lidar alerting algorithm of low-level wind shear based on ramps detection. *Infrared Laser Eng.* **2016**, *45*, 39–45. (In Chinese)
16. Jiang, L.; Zhao, L.; Xiong, X. The Gradient Search Alerting Algorithm of Low-level Wind Shear Based on Adaptive Scale. *Sci. Tech. Engrg.* **2015**, *15*, 1–6. (In Chinese)
17. Li, L.; Shao, A.; Zhang, K.; Ding, N.; Chan, P.W. Low-Level Wind Shear Characteristics and Lidar-Based Alerting at Lanzhou Zhongchuan International Airport, China. *J. Meteorol. Res.* **2020**, *34*, 633–645. [CrossRef]
18. Zhao, W.K.; Zhao, S.J.; Shan, Y.L.; Sun, X.J. Numerical Simulation for Wind Shear Detection with a Glide Path Scanning Algorithm Based on Wind LiDAR. *IEEE Sens. J.* **2021**, *21*, 20248–20257. [CrossRef]
19. Ricci, A.; Burlando, M.; Repetto, M.P.; Blocken, B. Simulation of urban boundary and canopy layer flows in port areas induced by different marine boundary layer inflow conditions. *Sci. Total Environ.* **2019**, *670*, 876–892. [CrossRef] [PubMed]
20. Woodfield, A.A.; Woods, J.F. *Worldwide Experience of Wind Shear during 1981–1982*; Royal Aircraft Establishment: Bedford, UK, 1983.
21. Li, H.; Ou, J. Spatiotemporal distribution characteristics of downburst in China. *J. Nat. Disasters* **2015**, *24*, 9–18. (In Chinese)
22. Liu, H.; He, M.; Wang, B.; Zhang, Q. Advances in low-level jet research and future prospects. *Acta Meteorol. Sin.* **2014**, *72*, 191–206. (In Chinese) [CrossRef]